

HOT-PRESSING OF QUARTZ POWDER TO  
.5 GPA PRESSURE AND 1250°C

by

RAYMOND JOSEPH HARPIN

B.A., University of Massachusetts  
(1972)

SUBMITTED IN PARTIAL FULFILLMENT  
OF THE REQUIREMENTS FOR THE  
DEGREE OF

MASTER OF SCIENCE

at the

MASSACHUSETTS INSTITUTE OF TECHNOLOGY

January 1980

© Massachusetts Institute of Technology 1980

Signature of Author

Department of Earth and  
Planetary Sciences  
January 22, 1980

Certified by

W.F. Brace  
Thesis Supervisor

Accepted by

Lindgren

MASSACHUSETTS INSTITUTE  
OF TECHNOLOGY

T. Madden  
Chairman

MAR 3 1980

Departmental Graduate Committee

LIBRARIES

HOT-PRESSING OF QUARTZ POWDER TO  
.5 GPA PRESSURE AND 1250°C

by

RAYMOND JOSEPH HARPIN

Submitted to the Department of Earth and Planetary Sciences  
on January 31, 1980, in partial fulfillment of the require-  
ments for the Degree of Master of Science

ABSTRACT

Quartz powder with an average grain size of 5  $\mu\text{m}$  (40  $\mu\text{m}$  to submicron size) was hot-pressed under hydrostatic gas pressures of 200 to 500 MPa and temperatures between 870 and 1250°C. The pore pressure was either 1 atm air, "dry conditions", or 100 MPa  $\text{H}_2\text{O}$ , "wet conditions".

The stress exponent,  $n$ , was determined to be  $1.9 \pm .3$  at 1250°C and  $1.9 \pm 1.5$  at 982°C. The apparent activation energy,  $Q_{\text{app}}$ , was determined to be  $40 \pm 20$  Kcal/mole for dry conditions in the temperature range stated above. No grain growth was observed. The volumetric strain rate under wet conditions was 25 times faster than under dry conditions.

The above creep parameters are only estimates of the creep parameters for fully dense quartz due to the approximate relation between volumetric strain rate,  $\dot{E}$ , in quartz powder and uniaxial strain rate,  $\dot{\epsilon}$ , in fully dense quartz. It is estimated that both diffusive and dislocation creep control densification of quartz powder under the conditions stated. The maximum density achieved was 88% theoretical density.

Thesis Supervisor: W.F. Brace

Professor of Geology

## ACKNOWLEDGMENTS

I wish to thank the following people for their assistance in this research project: Professor W.F. Brace, Dr. Brian Evans, Yves Caristan, Derek Hirst, Jane Palm, and Madge Slavin.

## TABLE OF CONTENTS

	<u>Page</u>
ABSTRACT .....	ii
ACKNOWLEDGMENTS .....	iii
TABLE OF CONTENTS .....	iv
LIST OF FIGURES .....	vi
LIST OF TABLES .....	vii
LIST OF SYMBOL DEFINITIONS .....	viii
Chapter	
I.    INTRODUCTION .....	1
1.1.  Introduction .....	1
1.2.  Theoretical Review of Hot-Pressing .....	2
II.   EXPERIMENTAL TECHNIQUE .....	7
2.1.  Sample Preparation .....	7
2.2.  The Experimental Apparatus .....	8
2.3.  Experimental Procedure .....	8
III.  RESULTS .....	13
3.1.  Graphs of $\dot{E}$ versus $\sigma$ for Raw Data .....	13
3.2.  Determination of $F(D)$ .....	13
3.3.  Effect of Temperature and Stress on the Densification Rate .....	18
IV.   DISCUSSION .....	26
4.1.  The Hot-Pressed Specimens .....	26
4.2.  Densification Curves .....	29
4.3.  Estimation of Creep Mechanisms .....	34

Chapter IV (contd.)	<u>Page</u>
4.4. Comparison of Hot-Pressing Parameters with those found for Deviatoric Creep of Fully Dense Solids .....	35
4.5. Experiments involving H <sub>2</sub> O Pore Pressure .....	36
4.6. Comparison of Experimentally-Determined $f(\bar{D})$ with theoretical formulations of $f(\bar{D})$ .....	37
V. CONCLUSIONS .....	39
APPENDIX I Magnitude of Surface Energy of Quartz Compared to Applied Pressure .....	40
II Comparison of $\dot{E}/f(\bar{D})_{\text{wet}}$ to $\dot{E}/f(\bar{D})_{\text{dry}}$ .....	41
III Diffusion Distance of H <sub>2</sub> O in Quartz at 300 MPa, 900°C .....	42
REFERENCES .....	46

## LIST OF FIGURES

## CHAPTER II

	<u>Page</u>
Figure 1 Specimen assembly for hot-pressing at 982°C .....	10

## CHAPTER III

Figure 2 Plot of $\dot{E}$ <u>vs</u> $\sigma$ at 1250°C .....	14
3 Plot of $\dot{E}$ <u>vs</u> $\sigma$ at 982°C .....	16
4 Plot of theoretical and experimental stress intensity functions, $f(D)$ , <u>vs</u> relative density, $D/D_{th}$ .....	19
5 Plot of $\dot{E}/f(\bar{D})$ <u>vs</u> $\sigma$ at 1250°C .....	21
6 Plot of $\dot{E}/f(\bar{D})$ <u>vs</u> $\sigma$ at 982°C .....	23

## CHAPTER IV

Figure 7 Scanning electron micrographs of fracture surfaces of specimens .....	27
8 Relative density, $D/D_{th}$ , <u>vs</u> time at 1250°C .....	30
9 Relative density, $D/D_{th}$ , <u>vs</u> time at 982°C .....	32

## LIST OF TABLES

	<u>Page</u>
Table 1    Theoretical Models of Hot-Pressing .....	43
Table 2    Experimental Data for Hot-Pressed Quartz ....	45

## LIST OF SYMBOL DEFINITIONS

$Q$	activation energy (Kcal/mole)
$Q_{app}$	apparent activation energy
$G$	grain diameter
$n$	stress exponent
$m$	grain-size exponent
$\sigma$	hydrostatic gas pressure
$\sigma_{eff}$	effective deviatoric stress ( $\sigma_{max} - \sigma_{min}$ )
$D$	density (gm/cm <sup>3</sup> or density of specimen/ 2.653 gm/cm <sup>3</sup> )
$\bar{D}$	average density ( $D_f - D_{in}/2$ )
$D_{in}$	density of specimen before experiment
$D_f$	density of specimen after experiment
$\dot{D}$	densification rate ( $\Delta D/\Delta t$ )
$T$	temperature
$t$	time
$\dot{E}$	volumetric strain rate ( $\dot{D}/D$ )
$\dot{\epsilon}$	uniaxial strain rate
$f(\bar{D})$	stress intensity function of average density = - 14.3( $\bar{D}$ ) + 12.5 at 1250°C = - 322.6( $\bar{D}$ ) + 259.4 at 982°C
$\dot{\epsilon}_{NH}$	Nabarro-Herring diffusional creep
$\Delta_L$	lattice diffusion coefficient of slowest moving species
$\Omega$	lattice vacancy volume
$k$	Boltzmann constant = $1.38 \times 10^{-23}$ joule/°K
$R$	gas constant = $1.98 \frac{\text{cal}}{\text{g}^\circ\text{K}}$
$\dot{\epsilon}_{C(B.D)}$	Coble or boundary diffusional creep
$\Delta_B$	boundary diffusion coefficient of slowest moving species
$\Delta_{DC}$	diffusion coefficient of dislocation climb
$\dot{\epsilon}_{DC}$	dislocation climb creep
$\mu$	shear modulus
$b$	Burger's vector
$\dot{\epsilon}_0, K$	pre-exponential constants



$K_D$	material constant called Dorn parameter
$\delta, W$	grain boundary thickness
$\sigma_Y$	flow strength of the material
$p$	pressure applied to outer shell
$\gamma$	surface energy
$r$	pore radius
$p_p$	pore pressure

## CHAPTER I

### INTRODUCTION

#### 1.1. Introduction

Hot-pressing is a technique used in metallurgy and ceramics (Kingery, 1976) to produce fine-grained, dense, polycrystalline materials from powders. The powder may be squeezed uniaxially in a stiff cylindrical die or, as in this study, squeezed hydrostatically inside thin ductile tubing (isostatic hot-pressing) which eliminates frictional forces between the compact and the die walls and results in truly hydrostatic stress being applied to the compact.

Hot-pressing has two important applications in rock mechanics. The first is to produce artificial "rocks" of controlled grain size and composition for further testing of physical properties previously done for creep (Nicolas et al., 1973), electrical conductivity (Duba, 1972; Dvorak, 1973; Bradley et al., 1964), and ultrasonic velocities (Anderson and Kanamori, 1968; Aherns et al., 1969). The second application is to use the densification rate of quartz in hot-pressing to determine deviatoric creep laws for deformation of single crystals, using the theoretical models of hot-pressing that have been proposed (Farnsworth and Coble, 1966; Murray et al., 1958; Coble, 1970; Rao and Chaklader, 1972; Wilkinson and Ashby, 1975; Notis et al.,

1975). These models give an approximate relation between densification rate and the deviatoric creep laws for the solid, so that estimates of the creep laws can be made from hot-pressing experiments.

Here we present densification rate, density, time, temperature, and compacting pressure for quartz powder (see Table 2). The temperature-pressure regime of the experiments was such that the quartz was in the B quartz field (Deer, Howie, and Zussman, 1966). A similar study has been done for olivine powder (Schwenn and Goetze, 1978).

## 1.2. Theoretical review of hot-pressing

To invert hot-pressing data to give information on solid state creep requires theoretical modelling of the hot-pressing process. Equations for densification from each model are listed in Table 1. Notice in Table 1 that the hot-pressing process is divided into three stages. The stages are defined as follows:

Stage	Pore geometry
1st stage	pores completely connected
2nd stage	pores are cylindrical in shape
3rd stage	pores are isolated spheres

In this study, SEM observations revealed that the specimens only reached the second stage of densification, so equations applying to the third stage will not be considered.

Each theoretical model must cover the following aspects of hot-pressing. Pressure is applied to the powder

specimen. Because there is some pore space around each grain, a deviatoric stress state is imposed on each grain which will cause solid state creep deformation in every grain. Actually, surface energy is also a driving force for deformation, but it is negligible in the case of quartz (see Appendix 1). As each grain deforms, the pore space in the whole powder specimen is reduced and the density,  $D$ , of the specimen increases.

The specific relations the models must define are:

(1) the relation between the applied pressure ( $\sigma$ ) and the deviatoric stress at the grain contacts ( $\sigma_{\text{eff}}$ ); (2) the relation between  $\sigma_{\text{eff}}$  and the rate of deformation at grain contacts (i.e. the constitutive equation of the deformation mechanism); (3) the relation between the deformation rate at grain contacts and the densification rate of the entire powder specimen. What follows is a general description of these relations used in all the hot-pressing theoretical models.

In determining the relation between the applied stress and the deviatoric stress, each model assumes the grains to be spheres of a uniform size arrayed in one of several packing configurations. The pressure applied is converted to a deviatoric stress at the contacts between grains. It is important to note that as the grains deform, the area of contact between grains increases. This reduces the  $\sigma_{\text{eff}}$  if the applied pressure ( $\sigma$ ) is held constant. Thus, the relation between  $\sigma$  and  $\sigma_{\text{eff}}$  is a function of the density of the

specimen, stated in equation form:

$$\sigma_{\text{eff}} = f(D) \sigma \quad (1.1)$$

Figure 4 is a graph of  $f(D)$  vs. density for several of the hot-pressing models as well as the  $f(\bar{D})$  determined from our hot-pressing experiments (see section 3.2).

The relation between  $\sigma_{\text{eff}}$  and deformation rate near the grain contacts is the creep law for the particular mechanism(s) assumed to be controlling the deformation. The three most significant mechanisms (Nabarro, 1948; Herring, 1950; Wilkinson and Ashby, 1975; Nicolas and Poirier, 1976; Coble, 1963; Notis et al., 1975; Bird et al., 1969; Weertman, 1968) are:

- (1) Nabarro-Herring diffusional creep, which is the result of vacancy motion through the bulk lattice along a stress-induced concentration gradient from grain boundaries in tension to boundaries in compression. The strain rate is expressed as:

$$\dot{\epsilon}_{\text{NH(L.D.)}} = \frac{13.3 \Delta_L \Omega \sigma_{\text{eff}}}{kTG^2} \quad (1.2)$$

- (2) Coble (boundary) diffusional creep, which is stress-directed diffusional flow along grain boundaries. The strain rate is expressed as:

$$\dot{\epsilon}_{\text{C(B.D.)}} = \frac{47.5 \delta \Delta_B \Omega \sigma_{\text{eff}}}{kTG^3} \quad (1.3)$$

- (3) Dislocation creep (power-law creep), where both stress and temperature are high enough so that

deformation is accomplished by both climb and glide of dislocations. A semi-empirical form for the creep rate is:

$$\dot{\epsilon}_{DC} = \frac{K_D \Delta_{DC} \mu^b}{\mu} \left( \frac{\sigma_{eff}}{\mu} \right)^n \quad (1.4)$$

$$n = 3 \text{ to } 5$$

A generalized form of the above three equations appropriate to the regime of low stress (below power-law breakdown) (Schwenn and Goetze, 1978; Goetze, 1978; Nicolas and Poirier, 1976) is:

$$\dot{\epsilon} = \dot{\epsilon}_0 (\sigma_{eff})^n G^{-m} \exp^{-Q/RT} \quad (1.5)$$

If  $n = 1$ , a diffusional process dominates.

If  $n = 3-5$ , power-law creep dominates.

The strain rate at the grain contacts can be directly converted to the volumetric strain rate (for small strains) by the equation:

$$\dot{E} = \frac{\dot{D}}{D} \rightarrow \dot{\epsilon} \quad (\text{Coble, 1970}) \quad (1.6)$$

In fully dense solids  $\dot{E} = 3\dot{\epsilon}$ , but there is only an approximate correspondence between the  $\dot{E}$  of hot-pressing and the  $\dot{\epsilon}$  of fully dense solids, because the solid state flow laws are based on the assumption that the grain boundary area and the diffusion path length remain constant (Coble, 1970). In hot-pressing these parameters do not remain constant.

The empirical densification law for hot-pressing is defined as:

$$\dot{E} = k f(\bar{D}) (\sigma)^n G^{-m} \exp^{-Q/RT} \quad (1.7)$$

It is of the same form as equation (1.5) for fully dense solids, but the experimentally-determined values of  $Q$  and  $n$  for equation (1.7) are only estimates of  $Q$  and  $n$  for solid state creep (equation (1.5)), for the reasons mentioned above. Since the determination of which mechanisms control the densification process is also based on  $Q$  and  $n$ , such a determination will be an estimate as well.

## CHAPTER II

### EXPERIMENTAL TECHNIQUE

#### 2.1. Sample Preparation

The quartz powder used was a commercially available product Sil-Co-Sil 400, produced by the Ottawa Silica Co., Ottawa, Illinois. It was a crushed quartz sand (99.8%  $\text{SiO}_2$ ) which had been passed through a #400 sieve, so the grain diameters range from 40  $\mu\text{m}$  down to submicron size with the average grain diameter being 5  $\mu\text{m}$ . This powder was used without further sieving.

To produce a powder specimen of desired density for an experiment, the powder was dried in a vacuum of 29" Hg, at a temperature of 400°C for several hours; then the powder was die-pressed, cold, in a cylindrical die under a load of 160 MPa for 30 seconds. This produced a cylindrical specimen of 1.7 cm. dia. x 2 cm. ht. with a density of 1.6  $\text{gm/cm}^3$  (60% theoretical density). The cold die-pressing also caused fracturing of the larger grains, reducing the largest grain diameter to about 20  $\mu\text{m}$  and the average grain diameter somewhat.

#### 2.2. The Experimental Apparatus

The hot-pressing was performed in a gas pressure



deformation apparatus which uses an external 1 GPa argon gas pumping system to generate pressure in the vessel. The specimen assembly for low temperature runs (982°C) is shown in Figure 1. For high temperature runs (1250°C) the copper tube was replaced by a tube whose upper end (over specimen) was platinum pulled onto the lower end, which was made of molybdenum. In a few initial high temperature runs (the H-H series in Table 2) the specimen was completely enclosed in a gas-tight platinum canister. In all the experiments a chromel-alumel thermocouple was in contact with the upper end of the specimen. In the "dry" experiments, except for the H-H series, the specimen was vented to the atmosphere through the opening seen in Figure 1. In the "wet" experiments (W series in Table 2) the specimen was exposed to 100 MPa of H<sub>2</sub>O pore pressure supplied by an external pumping system.

### 2.3. Experimental Procedure

After the cold die-pressing, each specimen was precision-ground to a right cylinder to enable accurate measurement of the initial density. The specimen was then hot-pressed at constant temperature and pressure for a given period of time and its final density measured in the same way as the initial density was measured.

Since densification rates were desired for specimens with an initial density of greater than .75 theoretical density, each specimen was hot-pressed twice - once to

increase the density beyond .75, and again to determine the densification rate.

Figure 1: Specimen assembly for hot-pressing at  
982°C

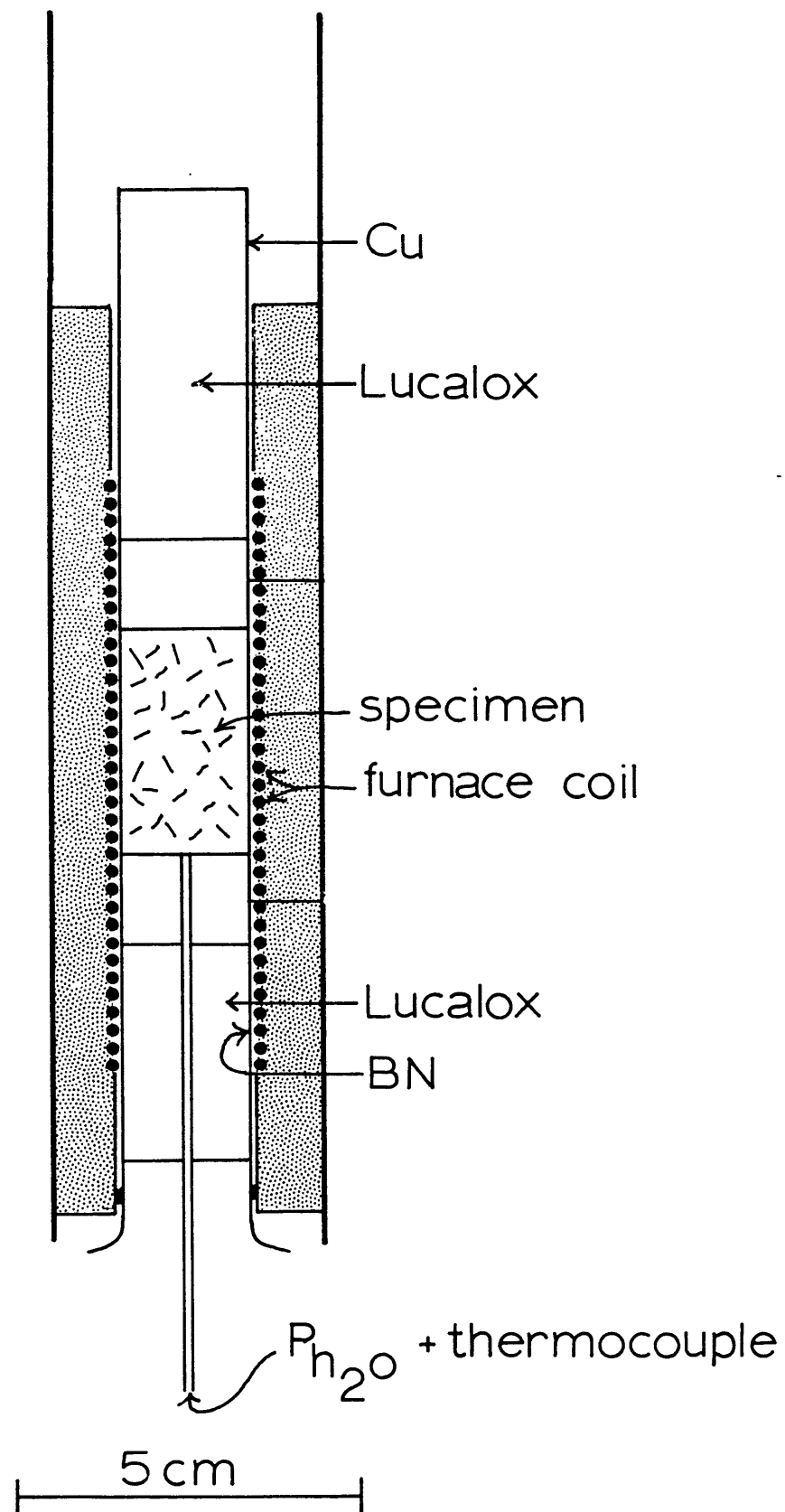


Figure 1

The density measurement had a maximum error of  $\pm .001 \text{ gm/cm}^3$ , but this error was increased to  $\pm .005 \text{ gm/cm}^3$  because the specimens swelled, presumably due to cracking caused by the introduction of water over a period of several days after the experiment. This error was reduced to a minimum by measuring sample density as soon as possible after each experiment. Other maximum errors were:

External pressure ( $\sigma$ ):  $\pm 1 \text{ MPa}$   
 Temperature:  $\pm 10^\circ\text{C}$   
 Time:  $\pm 5 \text{ min.}$

$\dot{E}$  was calculated as follows:

$$\dot{E} = \frac{D_F - D_{in}}{D_{in}(t)} \quad (1.8)$$

The maximum errors involved in the calculation of  $\dot{E}$  were:

$$\begin{aligned} \frac{\Delta \dot{E}}{\dot{E}} &= \pm .08 && \text{for experiments at } 1250^\circ\text{C} \\ &= \pm .2 && \text{for experiments at } 982^\circ\text{C}, \\ &&& D_{in} = 2.08 \text{ gm/cm}^3 \\ &= \pm .71 && \text{for experiments at } 982^\circ\text{C}, \\ &&& D_{in} = 2.12 \text{ gm/cm}^3 \end{aligned}$$

## CHAPTER III

### RESULTS

#### 3.1. Graphs of $\dot{E}$ versus $\sigma$ for Raw Data

The data obtained from the experiments are compiled in Table 2 and plotted on log scales in Figure 2 for the high temperature experiments and Figure 3 for the low temperature experiments. In Figure 3 the data separate into three distinct groups, according to their initial density. It is clear that, for a given hydrostatic pressure ( $\sigma$ ), a lower initial density implies a higher volumetric strain rate ( $\dot{E}$ ). This was expected because  $\sigma_{\text{eff}}$  increases with decreasing density, as discussed in section 1.2.

#### 3.2. Determination of $f(D)$

$f(D)$  depends on such geometrical factors as the average number of nearest neighbors, average contact area of grain-to-grain contacts, etc. (Farnsworth and Coble, 1966; Rao and Chaklader, 1972; McClelland, 1961; Spriggs and Vasilos, 1964). Rather than adopt a particular model developed for geometrical arrays of uniform spheres, an empirical determination of  $f(D)$  was used and is developed below.

For constant  $\sigma$ ,  $T$ , and  $G$ , equation 1.7 can be simplified by including  $(\sigma)^n$ ,  $G^{-m}$ , and the exponential term with the constant  $K$ , giving:

Figure 2: Plot of  $\dot{E}$  vs  $\sigma$  (gas pressure)  
on log scales at  $T = 1250^\circ\text{C}$ .  
Points are raw data from Table 2.  
Error bar shown is for all  
points.

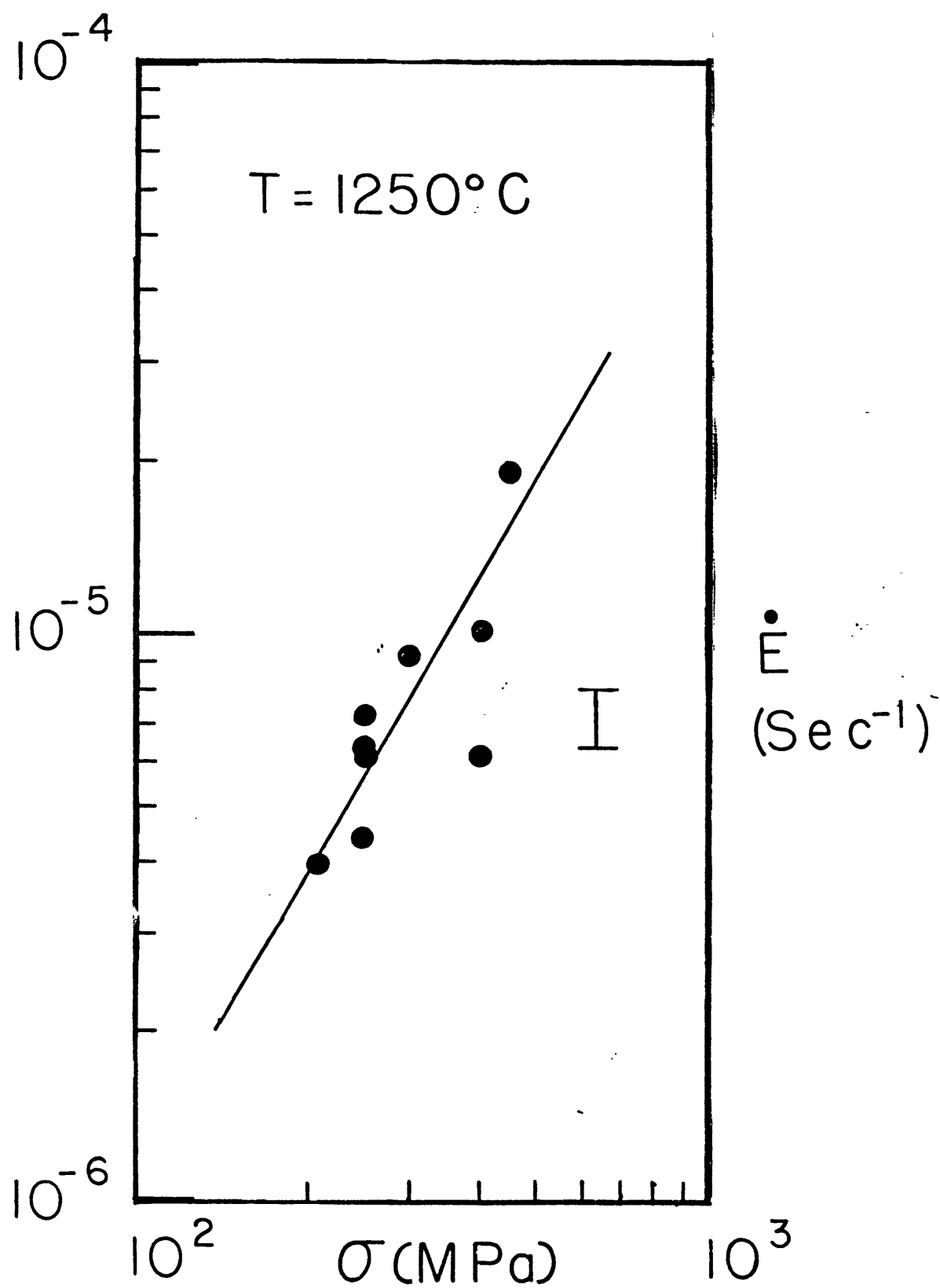


Figure 2



Figure 3: Plot of  $\dot{E}$  vs  $\sigma$  (gas pressure)  
on log scales at  $T = 982^\circ\text{C}$ . Points  
are raw data from Table 2.

▲ = runs with  $D_{\text{in}} \approx 2.12$

● = runs with  $D_{\text{in}} \approx 2.08$

◻ = runs with  $D_{\text{in}}$  averaged at  $\approx 2.04$

Lines are drawn through points of  
 $D_{\text{in}} = 2.08$  and  $D_{\text{in}} = 2.13$  to show  
variation of  $\dot{E}$  with density. Error  
bar on triangle for all triangles,  
error bar on circle for all circles.

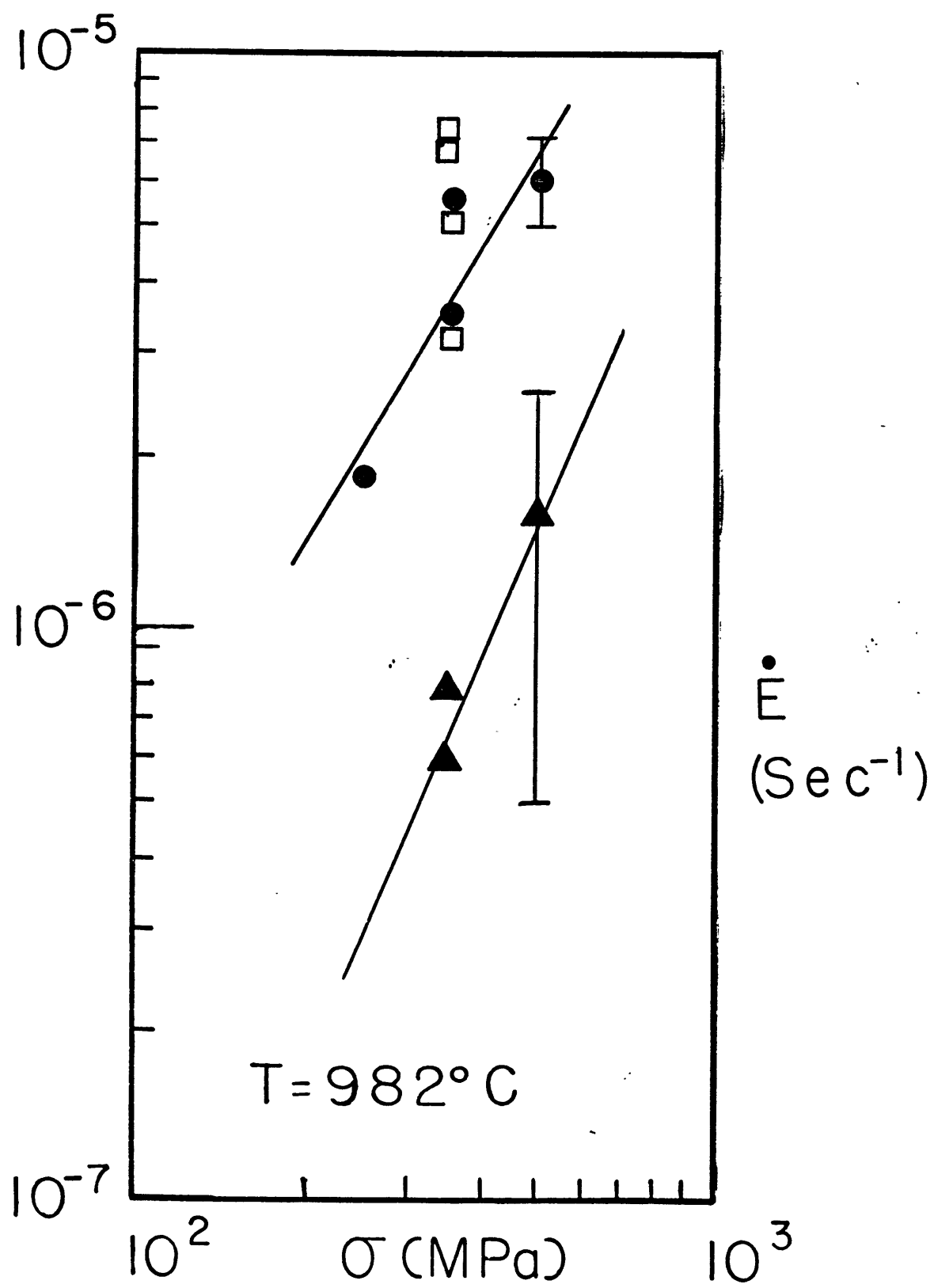


Figure 3

$$\dot{E} = K/\sigma, T, G f(\bar{D}) \quad (3.1)$$

where  $\bar{D} = \frac{D_f - D_{in}}{2}$  (average density)

If  $f(\bar{D})$  is chosen to be 1.0 for a particular density ( $D_o$ ),  $K$  is determined absolutely from the densification rate, and for any other density  $\bar{D}$ ,  $f(\bar{D}_1)$  is simply

$$f(\bar{D}_1) = \frac{\dot{E}_1}{\dot{E}_o} f(\bar{D}_o) = \frac{\dot{E}_1}{\dot{E}_o} \quad \text{const. } \sigma, T, G \quad (3.2)$$

providing that  $\sigma$ ,  $T$ , and  $G$  remain constant. The values of  $f(\bar{D})$  normalized to  $f(\bar{D}_o = .8 D_{\text{theoretical}})$  are shown in Figure 4 and are compared with theoretical predictions mentioned in Figure 4.

The volumetric strain rate can then be corrected for the effect of density by dividing by the appropriate linearly interpolated  $f(\bar{D})$  values (see Table 2). The adjusted  $\dot{E}/f(\bar{D})$  vs  $\sigma$  curves are plotted in Figures 5 and 6.

### 3.3. Effect of Temperature and Stress on the Densification Rate

By putting equation (1.7) in the form

$$\frac{\dot{E}}{f(\bar{D})} = K \sigma^n \exp(-Q/RT) \quad (3.3)$$

the apparent activation energy ( $Q_{\text{app}}$ ) and effective stress exponent ( $n$ ) can be determined by rearranging equation (3.3):

$$Q_{\text{app}} = -R \frac{\ln \frac{\dot{E}_1}{f(\bar{D}_1)} - \ln \frac{\dot{E}_2}{f(\bar{D}_2)}}{\left(\frac{1}{T_1} - \frac{1}{T_2}\right)} \quad \text{at const. } \sigma \quad (3.4)$$

Figure 4: Plot of stress intensity function,  $f(\bar{D})$ , normalized to  $f(D_o = 0.8 D_{\text{theoretical}}) = 1$  vs relative density  $(D/D_{\text{th}})$ . The continuous curves have been derived from the various hot-pressing models proposed for the effective stress,  $\sigma_{\text{eff}}$ , causing deformation during hot-pressing. The solid circles are the experimentally-determined  $f(\bar{D})$  from this study. The models represented are:

- (A) 1. McClelland (1961):  $f(D) = (1 - v_p^{\frac{2}{3}})^{-1}$   
 where  $p = 1-D$   
 2. Spriggs et al. (1964):  $f(D) = (1 + 2 v_p)$   
 3. Farnsworth and Coble (1966):  $f(D) = 1/D_{\text{rel}}$

(B,C,D,E) Rao and Chaklader (1972):  
 $f(D) = [\alpha_1 (D^{\frac{2}{3}} \beta^{\frac{2}{3}} R^2 - 1)]^{-1}$  where  $\alpha_1$  and  $\beta$  are geometric constants whose values depend upon the packing assumed; and  $R$  is the grain radius. These models suggest that  $\sigma_{\text{eff}}$  can be computed from the deformational geometries of the grains in contact. The four packing geometries assumed are: (B) cubic, (C) orthorhombic, (D) b.c.c., and (E) rhombohedral.

The upper error bar is for those circles above  $f(\bar{D}) = 1$ , the lower error bar for those below  $f(\bar{D}) = 1$ .

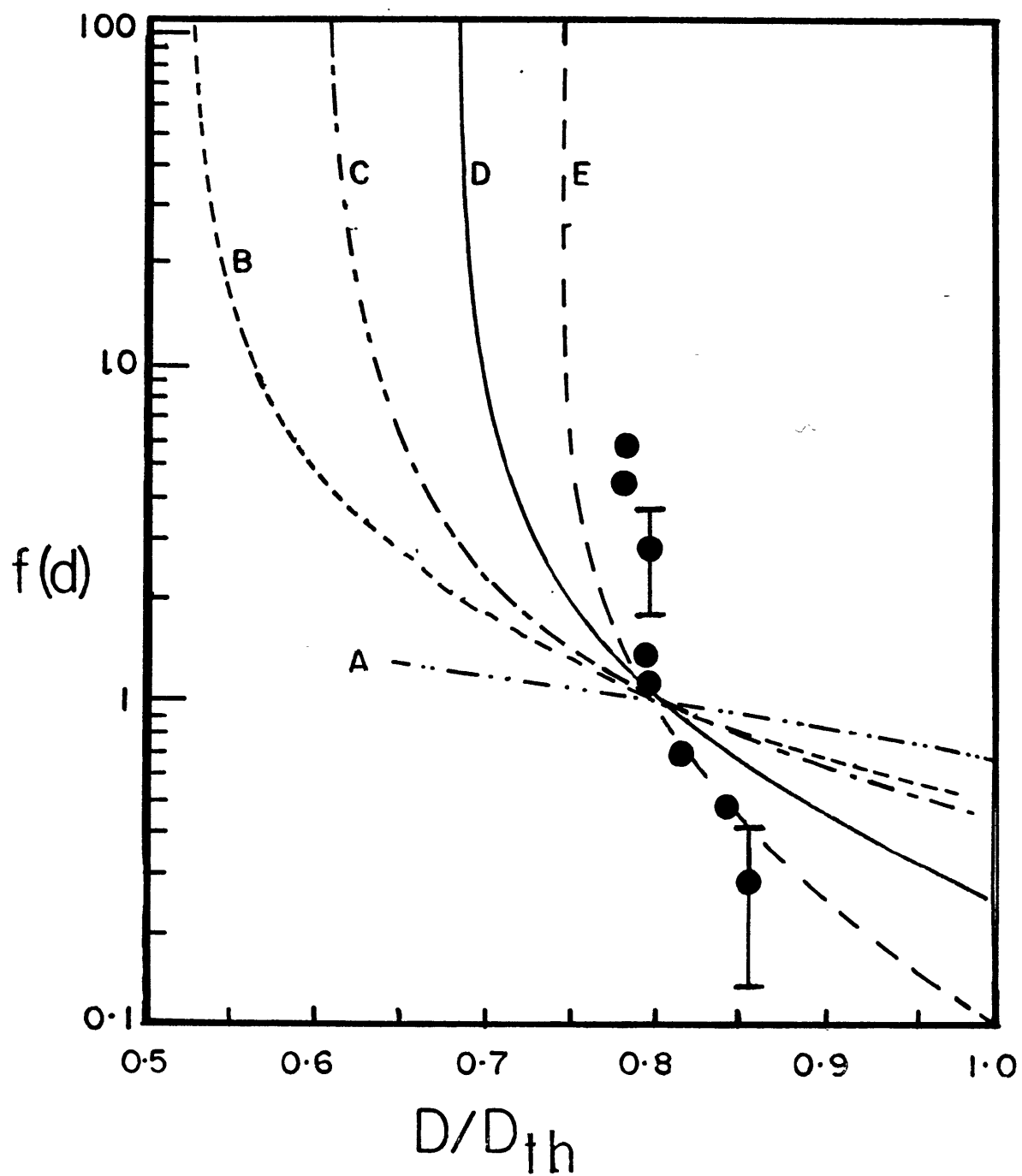


Figure 4

Figure 5; Plot of  $\dot{\epsilon}/f(\bar{D})$  vs  $\sigma$  (gas pressure)  
on log scales at  $T = 1250^\circ\text{C}$ .  
Points are from Table 2.

● = P series experiments (see Table 2)

□ = HH series experiments (see Table 2)

Line is least square fit of P series  
data. Stress exponent (n) = 1.9.

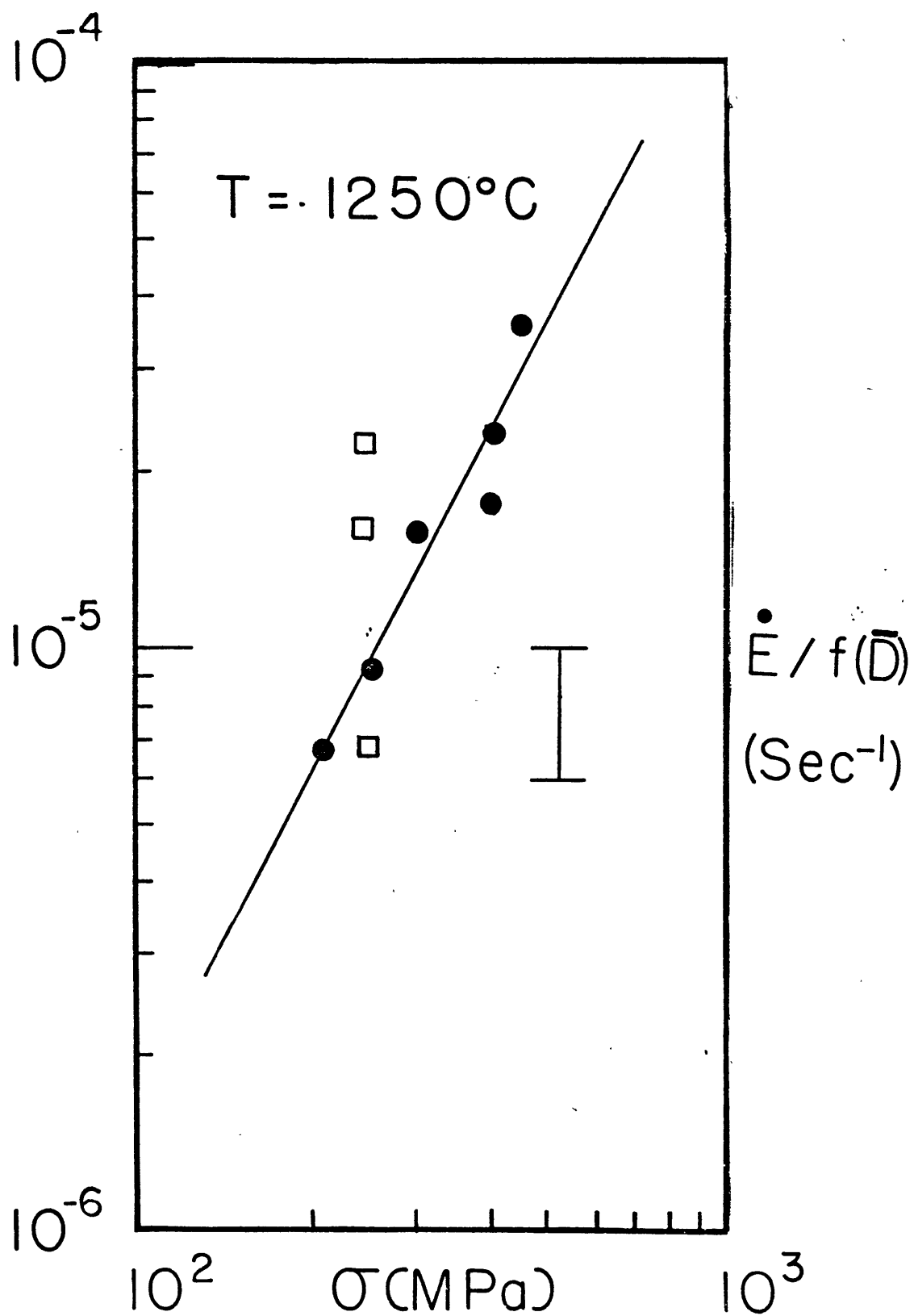


Figure 5

Figure 6: Plot of  $\dot{E}/f(\bar{D})$  vs  $\sigma$  (gas pressure) on log scales at 982°C. Points are from Table 2.

● = runs with  $D_{in} \approx 2.08$

▲ = runs with  $D_{in} \approx 2.12$

□ = runs not included in least square fit line. Line is least square fit of triangles and circles.  
 Stress exponent (n) = 2.0  
 Error bar on triangle is for all triangles. Error bar on circle is for all circles.



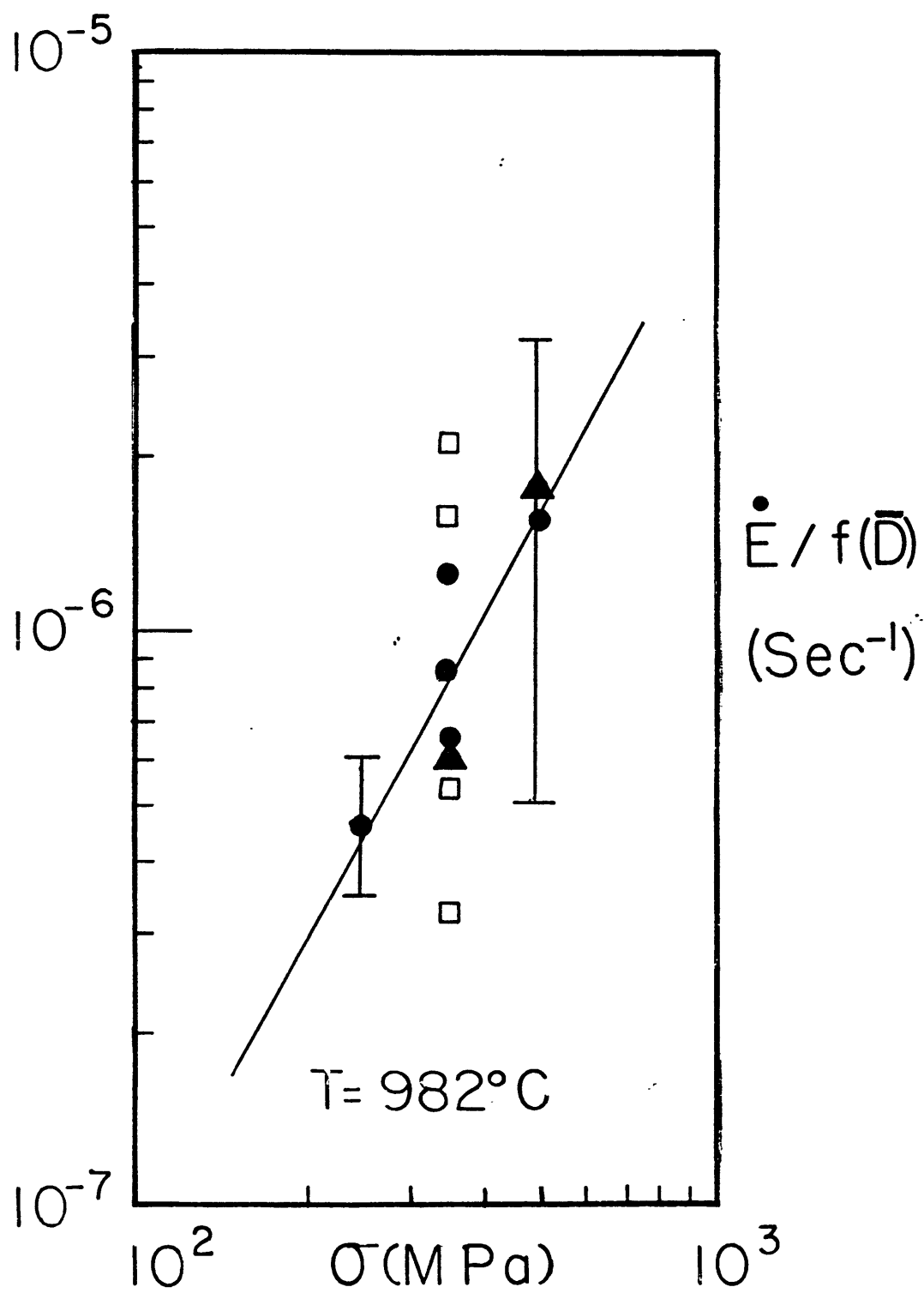


Figure 6

$$\text{and } n = \frac{\log \frac{\dot{E}_1}{f(\bar{D}_1)} - \log \frac{\dot{E}_2}{f(\bar{D}_2)}}{\log \sigma_1 - \log \sigma_2} \text{ at const. } T \quad (3.5)$$

The values determined are:

$$Q = 43 \text{ kcal/mole} \pm 20$$

$$n = 1.9 \pm .3 \text{ at } 1250^\circ\text{C}$$

$$n = 1.9 \pm 1.5 \text{ at } 982^\circ\text{C}$$

The large errors are due to small changes in density with respect to initial density at low temperatures. The significance of these values is discussed in the next chapter.

## CHAPTER IV

## DISCUSSION

4.1. The Hot-Pressed Specimens

Using thin sections and scanning electron micrographs, several qualitative observations concerning the hot-pressed specimens were made:

- (1) There was a much higher degree of wavy extinction in the larger grains (as seen from optical observations with crossed polarizers) in the hot-pressed specimens than in the undeformed powder, indicating at least some plastic deformation by dislocation motion in at least those grains. However, not all grains exhibit wavy extinction, which probably indicates that the geometry of the packing unevenly distributes the applied stress over all the grains. The microstructure of the smaller grains could not be determined optically.
- (2) SEM observation of a specimen which was unheated but cold-pressed at 500 MPa revealed grains with angular edges (Figure 7a), whereas the "dry" hot-pressed specimens (Figure 7b, 7c) have flattened edges but are still "subangular" in shape. The "wet" specimen (Figure 7d) shows almost no angularity. Furthermore, almost complete densification has occurred where small grains are in contact with other grains, small or

Figure 7: Scanning electron micrographs of fracture surfaces of specimens.

- (a) 10  $\mu\text{m}$  bar indicates scale, 500 MPa pressure, room temperature, 2 hr.
- (b) 1  $\mu\text{m}$  bar indicates scale, 350 MPa pressure, 982°C temperature, 2 hr.
- (c) 1  $\mu\text{m}$  bar indicates scale, 450 MPa pressure, 1250°C temperature, 1 hr.
- (d) 1  $\mu\text{m}$  bar indicates scale, 350 MPa pressure, 1000°C temperature, 5 min., 100 MPa pore pressure.

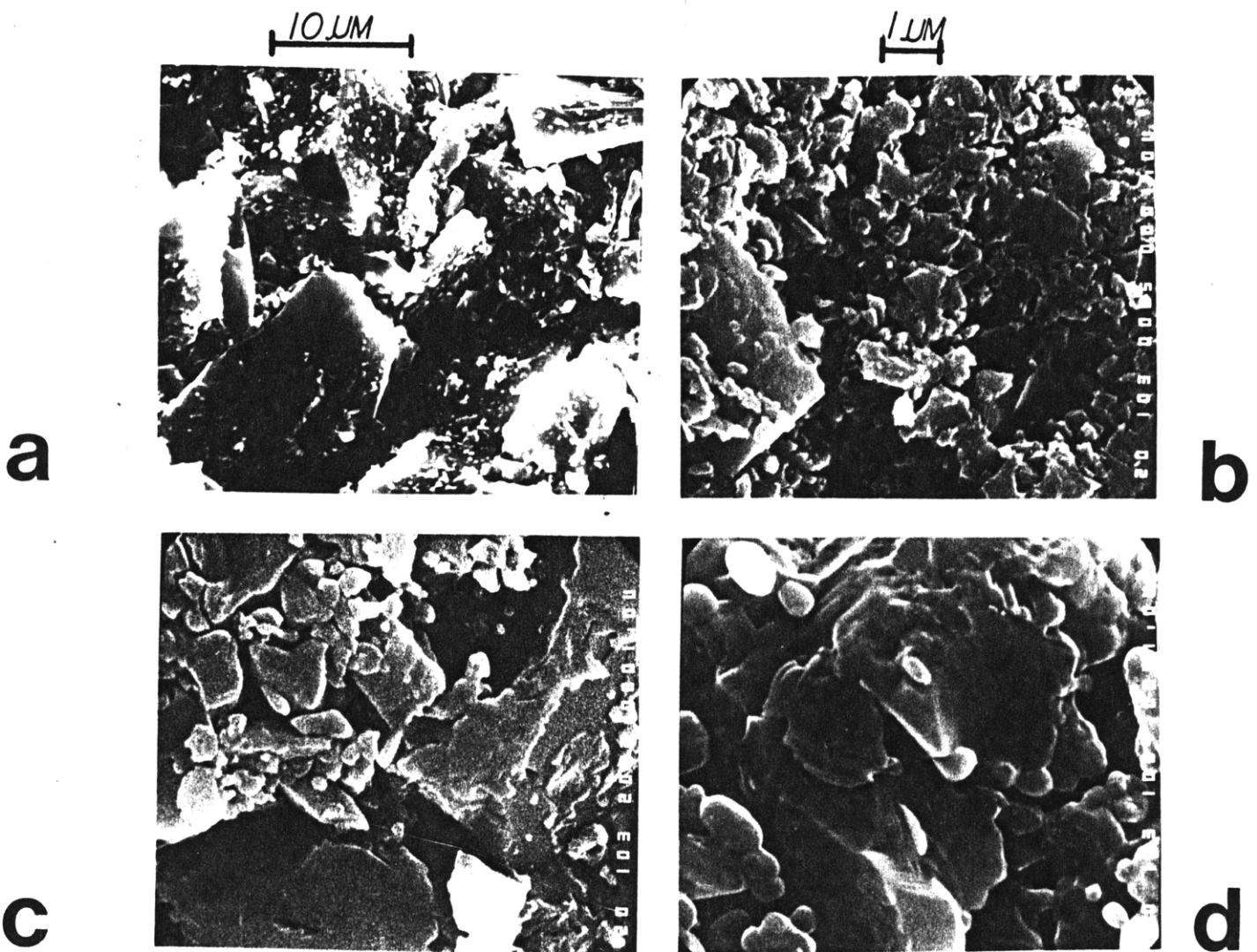


Figure 7

large. Porosity exists only between large grains. This would indicate that most of the deformation is occurring near the surface of each grain. One can also see considerable rounding of grain surfaces not in mechanical contact with other grains. This implies either rapid dissolution of quartz or markedly increased surface diffusion rates, as opposed to dry conditions. This striking difference is all the more remarkable since the time at temperature was only five minutes in the wet, as opposed to one hour in the dry.

- (3) No grain growth was observed in any of the dry experiments, which agrees with experimental observations made by Hobbs (1968).

#### 4.2. Densification Curves

Density vs time curves are useful for (1) designing future experiments to achieve a particular density, given a starting density, and (2) checking the consistency of the  $f(\bar{D})$  equations. Using the empirically-determined  $f(D)$  equations, density vs time curves can be constructed for different  $\sigma$  and  $T$  (Figures 8, 9). In these figures the lines are the densification curves based on  $f(\bar{D})$  and the points are the initial and final densities of the various experiments. In each case the initial density point is fitted to the curve corresponding to the correct  $\sigma$  at the point which corresponds

Figure 8: Plot of relative density ( $D/D_{th}$ ) vs time ( $t$ ) for  $\sigma = 400, 300, 250$  MPa and  $T = 1250^\circ\text{C}$ . The curves are calculated using  $f(\bar{D}) = -14(\bar{D}) + 12$ . Symbols that are the same indicate  $D_{in}$  and  $D_f$  for a given experiment.  $D_{in}$  is plotted on the curve according to its density, and  $D_f$  is plotted according to its density and  $\Delta t$  after  $D_{in}$  corresponding to duration of experimental run. Points are from Table 2.

Figure 8

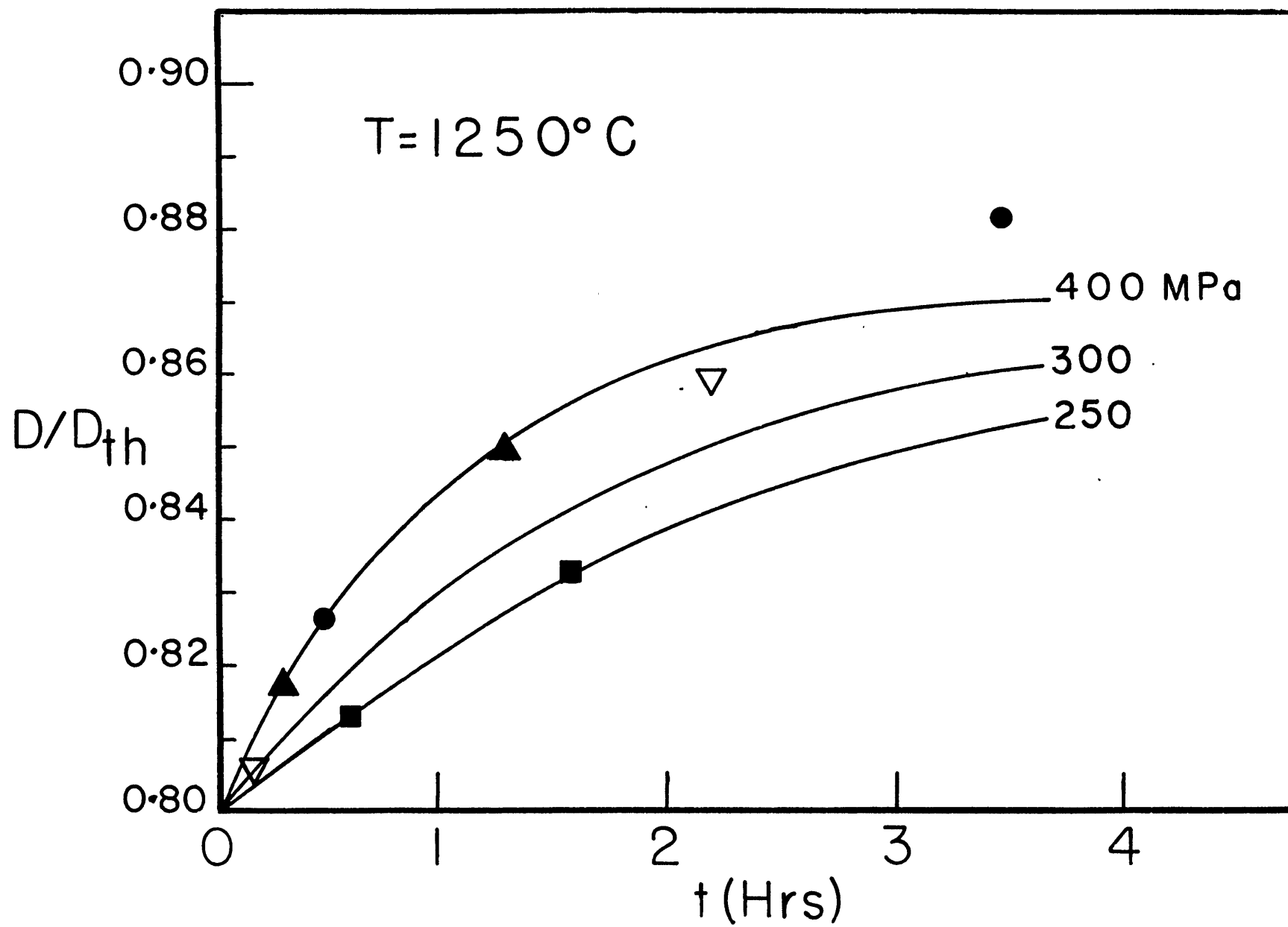
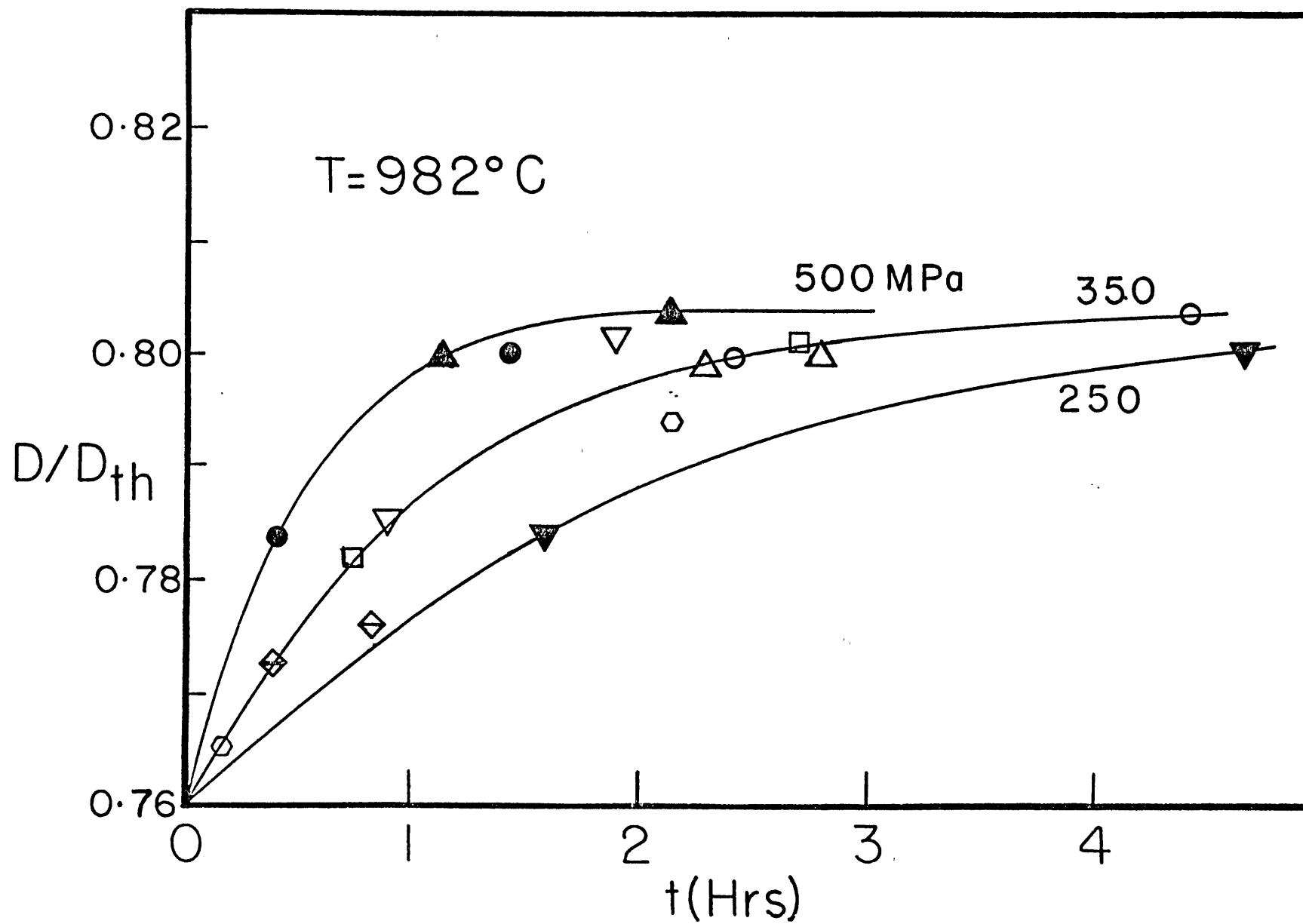




Figure 9: Same plot as Figure 8, except  
that here  $T = 982^{\circ}\text{C}$  and  $f(\bar{D}) =$   
 $- 323(\bar{D}) + 260.$

Figure 9



to the initial density. The final density point is plotted as its density at a  $\Delta t$  after  $D_{in}$ , corresponding to the duration of the experiment.

As seen from the figures, there is a reasonable fit between the curves and the data points.

#### 4.3. Estimation of Creep Mechanisms

As stated in section 1.2, there is only an approximate correspondence between  $\dot{E}$  for hot-pressing and  $\dot{\epsilon}$  for solid state creep. Therefore, the parameters determined from hot-pressing give only an estimate of those for creep in fully dense materials. The general densification rate equation for this study is:

$$\dot{E} = (2.55 \pm .5) f(\bar{D}) \sigma^{1.9 \pm 1.5} \exp\left(\frac{-43\text{kcal/mole} \pm 20}{RT}\right) \quad (4.1)$$

The parameters of the above equation do give an estimate of which creep mechanism(s) is(are) dominating the deformation. The value of 2.0 for this study suggests that the present experimental temperature-pressure regime is one of transition between diffusion dominance and dislocation creep dominance (Wilkinson and Ashby, 1975; Nicolas and Poirier, 1976). It would, however, be incorrect to assume that the same proportion of control by these two mechanisms would exist for the same pressure-temperature regime for creep of fully dense solids. Coble (1976) indicates that hot-pressing tends to enhance the relative importance of diffusional mechanisms so that

dislocation creep can be expected to have a greater role in creep of fully dense solids under the same conditions.

It should be further noted that the large variation in grain size in the hot-pressing experiments complicates the analysis. It may well be that diffusion is dominating in the smaller grains while dislocation climb dominates in the larger grains, as suggested by the optical and SEM observations.

In addition to errors arising from the empirical determination of  $f(\bar{D})$ , it must be remembered that the value of  $Q$  may be constantly changing if the experiments are being carried out in a region of transition between deformation mechanisms. In this case  $Q_{app}$  probably represents a weighted average of the activation energies of the competing mechanisms.

#### 4.4. Comparison of Hot-Pressing Parameters with those found for Deviatoric Creep of Fully Dense Solids

The value of  $Q$  for dislocation creep of "dry" quartz reported by several authors (Blacic and Griggs, 1965; Heard and Carter, 1968; Parrish et al., 1976; Christie et al., 1979; Carter, 1976) varies anywhere from 20 to 64 kcal/mole, while the value of  $Q$  for diffusion of oxygen is reported to be 55 kcal/mole (Haul and Dumbgen, 1962). Thus it can certainly be said that the  $Q_{app}$  of hot-pressing agrees in order of magnitude with  $Q$  for high temperature creep of "dry" quartz and with activation energies of diffusion of oxygen in quartz.

#### 4.5. Experiments involving H<sub>2</sub>O Pore Pressure

Since density measurements could be made on only one specimen run under wet conditions (W-2 in Table 2), the results will be discussed in qualitative terms.

From extrapolated values of  $\dot{E}/f(\bar{D})$  under dry conditions compared with  $\dot{E}/f(\bar{D})$  under wet conditions, the water increased the volumetric strain rate by a factor of twenty-five (Appendix 2). This is a very rough estimate, but there certainly was a sizeable increase in the rate. Two reasons for water increasing the deformation rate are by (1) diffusing into the crystalline structure of quartz and facilitating plastic deformation by movement of dislocations (hydrolytic weakening) (Griggs and Blacic, 1964; Griggs, 1967, 1974; Griggs et al., 1966; McLaren and Retchford, 1969), and (2) increasing the diffusion rate of silicon and/or oxygen, allowing accelerated diffusional creep.

Using the value of the diffusion constant for water in quartz, an estimate of diffusion distance for experiment W-1 (Table 2) is 0.035  $\mu\text{m}$  (Appendix 3). This precludes large-scale dislocation weakening in the center of grains larger than a micron. However, accelerated dislocation motion near the grain contacts could still occur.

Comparing the SEM picture of the "wet" (Figure 2d) vs the "dry" (2c, 2d) runs, several differences stand out. First, the grains are much more rounded in the wet run, even in those cases where the grains have little mechanical contact with

others. This certainly indicates that either surface diffusion or dissolution has been enhanced by water. Secondly, there is a much higher degree of densification where smaller grains are in contact with other small or large grains, as compared to the dry runs. Finally, there does not seem to be a noticeable difference in the amount of densification between large grains, from wet to dry conditions, as judged from grain flattening and neck size.

The fact that densification is more rapid for smaller grain sizes suggests that diffusional processes are accelerated in the wet runs, since  $\dot{\epsilon} \propto G^{-2}$  or  $3$  for diffusional creep while dislocation creep is grain-size insensitive.

Taken by itself this evidence is only suggestive and far from conclusive. However, it does seem that enhancement of diffusion processes vis-à-vis dislocation processes is at least a possibility under wet conditions.

#### 4.6. Comparison of Experimentally-Determined $f(\bar{D})$ with Theoretical Formulations of $f(\bar{D})$

Figure 4 shows the effective stress function,  $f(D)$ , from theoretical models of various geometrical packings of uniform spheres compared to our experimentally-determined data. Going from curve A through E (Figure 4), there is an increase in the sensitivity of  $f(D)$  to density, and also an increase in the density of the packing. It is the increasing number of contacts with other spheres that causes the increasing sensitivity of  $f(\bar{D})$  to density. The experimentally-determined

effective stress function is more sensitive to density than any of the theoretical curves. This is probably due to an even greater number of contacts between grains in the quartz powder, compared to the most compact packing model. The denser packing of the powder is the result of a range of grain sizes rather than one size being present.

## CHAPTER V

## CONCLUSIONS

- (1) The quartz powder had a stress exponent,  $n$  of  $1.9 \pm 0.3$  at  $1250^{\circ}\text{C}$  and  $1.9 \pm 1.5$  at  $982^{\circ}\text{C}$ .
- (2) The apparent activation energy,  $Q_{\text{app}}$ , was  $43 \pm 20$  kcal/mole in the range of  $982^{\circ}\text{C}$ - $1250^{\circ}\text{C}$  and 200-500 MPa.
- (3) The maximum density achieved was 88% theoretical density.
- (4) Under "wet" conditions the specimens densified about twenty-five times faster than under "dry" conditions.
- (5) No grain growth was observed in any experiments.



## APPENDIX I

Magnitude of Surface Energy of Quartz  
Compared to Applied Pressure

$$(1) \quad \gamma_{(\text{max qtz})} = 1,030 \text{ erg/cm}^2 \quad (\text{Brace and Walsh, 1962})$$

$\gamma$  = surface energy

(2) Driving force term containing surface energy is:

$$\frac{\gamma}{r} \quad \text{where } r = \text{radius of pore} \quad (\text{Coble, 1970})$$

Assume  $r = 1 \text{ } \mu\text{m} = 10^{-4} \text{ cm}$

(3) Therefore

$$\frac{\gamma}{r} = \frac{1030 \text{ dyne cm/cm}^2}{1 \times 10^{-4} \text{ cm}} = 1.03 \times 10^7 \text{ dyne/cm}^2$$

$$\frac{\gamma}{r} = 1.03 \text{ MPa}$$

(4) Compared to an applied stress of 250 MPa, 1.03 MPa is negligible, so the surface energy term can be neglected.

## APPENDIX II

Comparison of  $\dot{E}/f(\bar{D})_{\text{wet}}$  to  $\dot{E}/f(\bar{D})_{\text{dry}}$

- (1) Determine what  $\dot{E}/f(\bar{D})_{\text{dry}}$  would be under the pressure, temperature conditions used in the wet run ( $T = 872^\circ\text{C}$ ,  $\sigma = 350 \text{ MPa}$ ,  $PP = 100 \text{ MPa}$ )
- (2)  $\sigma_{\text{eff}} = \sigma_{\text{app}} - PP = 250 \text{ MPa}$
- (3) Assume  $Q_{\text{dry}}$  remains constant at 43 kcal/mole
- (4) Rearranging equation 3.8 gives:

$$\dot{E}_{2/f}(\bar{D}_1) = \exp\left[\frac{Q}{R} \cdot \left(\frac{1}{T_1} - \frac{1}{T_2}\right)\right] + \ln \dot{E}_{1/f}(\bar{D}_2)$$

where  $\dot{E}_{1/f}(\bar{D}_1)$  = adjusted volumetric strain rate of dry quartz at 250 MPa,  $982^\circ\text{C}$

$$\dot{E}_{1/f}(\bar{D}_1) = 4.65 \times 10^{-7} \text{ sec}^{-1}, T = 982^\circ\text{C}, T = 872^\circ\text{C}$$

$\dot{E}_{2/f}(\bar{D}_2)$  = adjusted extrapolated volumetric strain rate of dry quartz

Results:

$$\dot{E}_{2/f}(\bar{D}_2) = 8.8 \times 10^{-8} \text{ is 25 times slower than}$$

$$\dot{E}/f(\bar{D}_1)(\text{wet}), \text{ which equals } 2.17 \times 10^{-6} \text{ sec}$$

## APPENDIX III

Diffusion Distance of H<sub>2</sub>O in Quartz

at 300 MPa, 900°C

$$\text{Distance} = \sqrt{2\Delta_{\text{H}_2\text{O}} t} \quad (\text{Paterson and Kekulawala, 1979})$$

$$\Delta_{\text{H}_2\text{O}} = \text{diffusivity of water} = 10^{-18} \text{ m}^2/\text{sec}$$

$$t_{\text{max}} = 10 \text{ min}$$

so

$$\text{Diffusion distance} = \sqrt{2(10^{-18} \text{ m}^2/\text{sec})(600 \text{ sec})}$$

$$= \underline{0.035 \text{ } \mu\text{m}}$$

TABLE I

Reference	Comments	Model	Creep mechanism
Wilkinson & Ashby, 1975	Second stage assumes cylindrical pores	$\dot{D}_1 = \frac{3D_2\Omega}{kTb^2} \frac{(1-D)^{\frac{1}{3}}}{1-(1-D)^{\frac{1}{3}}} P$ $\dot{D}_2 = \frac{9}{2} \frac{\delta D (B.D)^{\frac{1}{2}}}{kTb^3} \frac{1}{1-(1-D)^{\frac{1}{3}}} \sigma_{eff}$ $\dot{D}_3 = \frac{3}{2} \frac{SA}{[1-(1-D)^{\frac{1}{n}}]^n} \left( \frac{3l}{2n} \frac{\sigma_{eff}}{\sigma_y} \right)^n$ <p>note: <math>b \approx</math> outer shell radius</p> $D_{lim} = 1 - \exp\left(-\frac{3}{2} \frac{\sigma_{eff}}{\sigma_y}\right)$	Lattice diffusion  Boundary diffusion  Power law creep  Glide limited plastic flow
Murray, Livey & Williams (1958)	Final stage uses MacKenzie & Shuttleworth continuum sintering process - Newtonian viscosity	$\frac{dD}{dt} = \frac{9}{4} A \sigma_{eff} (1-D)$ $A = \frac{1}{3} \text{ viscosity}$	
Notis et al. (1975)	Final stage assumes closed spherical pores	$\dot{D} = \dot{\epsilon} \left(\frac{3}{2}\right)^{n+1} \left(\frac{G}{n}\right)^n \frac{D(1-D)}{[1-(1-D)^{\frac{1}{n}}]^n}$	Any mechanism
Coble (1970)	Initial stage	$16(\dot{E})^2 = (32\Delta_L \Omega / G^3 kT) [\gamma + (\sigma G / \pi)]$ $64(\dot{E}) = (96\Delta_b W \Omega / G^4 kT) (+ \sigma G / \pi)$	Lattice diffusion  Boundary diffusion

TABLE I (continued)

Reference	Comments	Model	Creep mechanism
Coble (1970) (contd.)	Intermediate stage spherical pores	$\dot{\epsilon} = (40 \Delta_L \Omega / 3G^2 kT) (\sigma/D + \frac{\gamma}{r})$ $\dot{\epsilon} = (47.5 \Delta_b W \Omega / G^4 kT) (Pa/D + \frac{\gamma}{r})$	Lattice diffusion  Boundary diffusion
	Final stage isolated spheri- cal pores	$\dot{\epsilon} = (40 \Delta_L \Omega / 3G^2 kT) (\sigma/D + 2\frac{\gamma}{r})$ $\dot{\epsilon} = (7.5 \Delta_b W / G^3 kT) (\sigma/D + 2\frac{\gamma}{r})$	Lattice diffusion  Boundary diffusion
Rao et al. (1972)	All stages	$\dot{\epsilon} = A \sigma^n$ (plastic flow) $= \frac{\dot{D}}{D} + A (\frac{\sigma_{eff}}{\sigma})^n$ where $\frac{\sigma_{eff}}{\sigma} = [\alpha_1 (D^{\frac{2}{3}} \beta^{\frac{2}{3}} R^2 - 1)]^{-1}$ R = particle radius D = relative density $\beta$ and $\alpha$ depend on packing	

TABLE 2

Run No.	Time hrs.	Temp. °C	Pressure MPa	D <sub>in</sub> g/cm <sup>3</sup>	D <sub>f</sub> g/cm <sup>3</sup>	$\dot{E}$ (sec gm/cm <sup>3</sup> ) <sup>-1</sup>	f( $\bar{D}$ )	$\dot{E}/f(d)$ (sec gm/cm <sup>3</sup> ) <sup>-1</sup>	Pore pressure
c-1	3.0	982	250	2.08	2.12	$1.83 \times 10^{-6}$	3.94	$4.65 \times 10^{-7}$	1 atm air
c-2	1.0	982	500	2.079	2.124	$6.01 \times 10^{-6}$	3.85	$1.56 \times 10^{-6}$	" " "
c-3	2.0	982	350	2.074	2.126	$3.48 \times 10^{-6}$	4.04	$8.61 \times 10^{-7}$	" " "
c-4	2.0	982	350	2.05	2.16	$7.4 \times 10^{-6}$	3.44	$2.15 \times 10^{-6}$	" " "
c-5	1.5	982	350	2.048	2.127	$7.14 \times 10^{-6}$	5.58	$1.28 \times 10^{-6}$	" " "
c-6	2.0	982	350	2.03	2.106	$5.2 \times 10^{-6}$	7.93	$6.55 \times 10^{-7}$	" " "
c-7	1.0	982	350	2.084	2.127	$5.6 \times 10^{-6}$	3.37	$1.66 \times 10^{-6}$	" " "
c-7A	2.0	982	350	2.121	2.130	$5.9 \times 10^{-7}$	.942	$6.26 \times 10^{-7}$	" " "
c-9	1.0	982	500	2.120	2.132	$1.57 \times 10^{-6}$	.882	$1.78 \times 10^{-6}$	" " "
c-10	0.5	982	350	2.047	2.059	$3.26 \times 10^{-6}$	9.76	$3.34 \times 10^{-7}$	" " "
c-11	0.5	982	350	2.120	2.123	$7.90 \times 10^{-7}$	1.43	$5.53 \times 10^{-7}$	" " "
P-1	2.0	1250	300	2.14	2.28	$9.09 \times 10^{-6}$	.57	$1.596 \times 10^{-5}$	" " "
P-2	1.0	1250	450	2.14	2.29	$1.95 \times 10^{-5}$	.54	$3.59 \times 10^{-5}$	" " "
P-4	1.0	1250	250	2.16	2.21	$6.43 \times 10^{-6}$	.70	$9.13 \times 10^{-6}$	" " "
P-5	1.0	1250	400	2.17	2.25	$1.02 \times 10^{-5}$	.57	$1.79 \times 10^{-5}$	" " "
P-7	3.0	1250	400	2.19	2.34	$6.16 \times 10^{-6}$	.26	$2.34 \times 10^{-5}$	" " "
P-8	3.9	1250	208	2.15	2.27	$3.95 \times 10^{-6}$	.58	$6.81 \times 10^{-6}$	" " "
H-H-1	1.0	1250	2.5	2.23	2.29	$7.2 \times 10^{-6}$	.32	$2.27 \times 10^{-5}$	?
H-H-2	3.0	1200	2.5	2.17	2.32	$6.4 \times 10^{-6}$	.38	$1.68 \times 10^{-5}$	?
H-H-3	4.0	1200	2.5	2.13	2.26	$4.5 \times 10^{-6}$	.65	$6.92 \times 10^{-6}$	?
W-1	.08	1000	3.5	1.98	-	-	-	-	100 MPa H <sub>2</sub> O
W-2	1.0	872	3.5	2.00	2.13	$1.81 \times 10^{-5}$	8.34	$2.17 \times 10^{-6}$	100 MPa H <sub>2</sub> O

## REFERENCES

- Aherns, T.J., D.L. Anderson, and A.E. Ringwood, Equation of state and crystal structures of high pressure phases of shocked silicates and oxides, Rev. Geophys., 7, 667-709, 1969.
- Anderson, D.L., and H. Kanamori, Shock-wave equations of state for rocks and minerals, J. Geophys. Res., 73, 6477-6503, 1968.
- Bird, J.E., A.K. Mukherjee, and J.F. Dorn, in Quantitative Relations Between Properties and Microstructure, D.G. Brandon and A. Rosen (eds.), p. 255, Israel Univ. Press, 1969.
- Blacic, J.D., and D.T. Griggs, New phenomena in experimental deformation of quartz at low strain rate (abstr.), EoS. Trans. AGU, 46, 541, 1965.
- Brace, W.F., and J.B. Walsh, Some direct measurements of the surface energy of quartz and orthoclase, Amer. Mineral., 47, 1111-1122, 1962.
- Bradley, R.S., A.K. Jamil, and D.E. Munro, The electrical conductivity of olivine at high temperatures and pressures, Geochim. Cosmochim., 28(11), 1669-1678, 1964.
- Carter, N.L., Steady-state flow of rocks, Rev. Geophys. Spec. Phys., 14(3), 326-327, 1976.

- Christie, J.M., P.S. Kock, and R.P. George, Flow law of quartzite in the alpha-quartz field (abstr.), EoS, Trans. AGU, 60(46), 948-949, 1979.
- Coble, R.L., A model for boundary diffusion-controlled creep in polycrystalline materials, J. Appl. Phys., 34(6), 1679-1682, 1963.
- Coble, R.L., Diffusional models for hot-pressing with surface energy and pressure effects as driving forces, J. Appl. Phys., 41(12), 4798-4807, 1970.
- Coble, R.L., The status of understanding diffusion-controlled solid state sintering, hot-pressing and creep, 8th Internatl. Sympos. on Reactivity of Solids, pp. 669-688, Plenum Press, New York, 1976.
- Deer, W.A., R.A. Howie, and J. Zussman, An Introduction to the Rock-Forming Minerals, Longman Group Ltd., London, p. 348, 1966.
- Duba, A., Electrical conductivity of olivine, J. Geophys. Res., 77, 2483-2495, 1972.
- Dvorak, Z., Electrical conductivity of several samples of olivines, peridotites, and dunites as a function of pressure and temperature, Geophysica, 38(1), 14-24, 1973.
- Farnsworth, P.L., and R.L. Coble, Deformation behavior of dense polycrystalline SiC, J. Amer. Ceram. Soc., 49, 264-268, 1966.



- Griggs, D.T., and J.D. Blacic, Quartz: anomalous weakness of synthetic crystals, Science, 147, 292-295, 1965.
- Goetze, C., The mechanisms of creep in olivine, Phil. Trans. Roy. Soc. Lond., A, 288, 99-119, 1978.
- Griggs, D.T., Hydrolytic weakening of quartz and other silicates, Geophys. J. Roy. astr. Soc., 14, 19-31, 1967.
- Griggs, D.T., A model of hydrolytic weakening in quartz, J. Geophys. Res., 79, 1653-1661, 1974.
- Griggs, D.T., and J.D. Blacic, The strength of quartz in the ductile regime (abstr.), EOS, Trans. AGU, 45, 102-103, 1964.
- Griggs, D.T., J.D. Blacic, J.M. Christie, A.C. McLaren, and F.C. Frank, Hydrolytic weakening of quartz crystals, Science, 152, 4, 1966.
- Haul, R., and G. Dumbgen, Investigation of oxygen diffusion in  $\text{TiO}_2$ , quartz and quartz glass by isotope exchange, Z. Elektrochem., 66, 636, 1962.
- Heard, H.C., and N.L. Carter, Experimentally induced "natural" intragranular flow in quartz and quartzite, Amer. J. Sci., 266, 1-42, 1968.
- Herring, C., Diffusional viscosity of a polycrystalline solid, J. Appl. Phys., 21, 437-445, 1950.

Hobbs, B.E., Recrystallization of single crystals of quartz,  
Tectonophysics, 6(5), 353-401, 1968.

Kingery, W.D., H.K. Bowen, and D.R. Uhlmann, Introduction  
to Ceramics, pp. 501-502, John Wiley & Sons, New York, 1976.

McLaren, A.C., and J.A. Retchford, Transmission microscope  
study of the dislocations in plastically-deformed synthetic  
quartz, Phys. Status Solidi, 33, 657-668, 1969.

McClelland, J.D., A plastic model of hot-pressing, J. Amer.  
Ceram. Soc., 44, 526, 1961.

Murray, P., D.T. Livey, and J. Williams, The hot-pressing of  
ceramics, Ceramics Fabrication Processes, W.D. Kingery  
(ed.), pp. 147-170, M.I.T. Press, Cambridge, 1958.

Nabarro, F.R.N., Report of a Conference on the Strength of  
Solids, Physical Soc., London, 75-90, 1948.

Nicolas, A., F. Boudier, and A.M. Bollier, Mechanisms of flow  
in naturally and experimentally-deformed peridotites,  
Amer. J. Sci., 273, 853-876, 1973.

Nicolas, A., and J.P. Poirier, Crystalline Plasticity and  
Solid State Flow in Metamorphic Rocks, John Wiley & Sons,  
New York, 1976.

Notis, M.R., R.H. Smoak, and V. Krishnamachari, Interpretation  
of hot-pressing kinetics by densification mapping  
techniques, Proc., 4th Interntl. Conf. on Sintering and  
Related Phenomena, 493-507, 1975.

- Parrish, D.K., A. Krivz, and N.L. Carter, Finite element folds of similar geometry, Tectonophysics, 32, 183-208, 1976.
- Paterson, M.S., and K.A.S.S. Kekulawala, The role of water in quartz deformation, Bull. Mineral., 102, 92-98, 1979.
- Rao, A.S., and A.C.D. Chaklader, Plastic flow during hot-pressing, J. Amer. Ceram. Soc., 55(12), 596-601, 1972.
- Schwenn, M.B., Creep of Olivine during Hot-Pressing, MS Thesis, M.I.T., Cambridge, 1965.
- Schwenn, M.B., and C. Goetze, Creep of olivine during hot-pressing, Tectonophysics, 48, 41-60, 1978.
- Spriggs, R.M., and R. Vasilos, Functional relation between creep rate and porosity for polycrystalline ceramics, J. Amer. Ceram. Soc., 47, 47-48, 1964.
- Weertman, J., Dislocation climb theory of steady-state creep, Trans. Amer. Soc. Met., 61, 681-694, 1968.
- Wilkinson, D.S., and M.F. Ashby, The development of pressure sintering maps, Proc., 4th Internat. Conf. on Sintering and Related Phenomena, 475-492, 1975.